



OPEN ACCESS

EDITED BY
Chitaranjan Pany,
Vikram Sarabhai Space Centre, India

REVIEWED BY
Xujiang Chao,
Northwestern Polytechnical University,
China
Katarzyna Michalowska,
SINTEF Digital, Norway

*CORRESPONDENCE
Yingxin Zhao,
✉ yxzhao15801042226@163.com

RECEIVED 02 December 2025
REVISED 03 February 2026
ACCEPTED 04 February 2026
PUBLISHED 05 March 2026

CITATION
Zhang H, Zhao Q, Zhao Y, Zhao B, Zhao M
and Liu C (2026) Data-driven wear
prediction method for complex
engineering structures.
Front. Mech. Eng. 12:1759085.
doi: 10.3389/fmech.2026.1759085

COPYRIGHT
© 2026 Zhang, Zhao, Zhao, Zhao, Zhao
and Liu. This is an open-access article
distributed under the terms of the [Creative
Commons Attribution License \(CC BY\)](#).
The use, distribution or reproduction in
other forums is permitted, provided the
original author(s) and the copyright
owner(s) are credited and that the original
publication in this journal is cited, in
accordance with accepted academic
practice. No use, distribution or
reproduction is permitted which does not
comply with these terms.

Data-driven wear prediction method for complex engineering structures

Haibo Zhang¹, Qingyuan Zhao¹, Yingxin Zhao^{1*}, Baiyang Zhao^{1,2},
Meng Zhao³ and Chuang Liu³

¹Standards & Metrology Research Institute, China Academy of Railway Sciences Corporation Limited, Haidian, Beijing, China, ²China Railway Test & Certification Center Limited, Beijing, China, ³College of Civil Engineering, Nanjing Tech University, Nanjing, China

Predicting the evolution of wear in metallic structural components is vital for accurately estimating the lifetime of engineering equipment. However, this remains a significant challenge due to the prohibitively large number of cycles required for traditional experiments or simulations. To address this, we established a data-driven approach to predict metal wear evolution during dynamic mechanical interactions. Our methodology involves two main steps: developing a high-fidelity finite element (FE) model to accurately simulate the wear, and then training a deep learning model that uses applied loads and historical wear data to predict future wear evolution. We selected contact wire clips in a high-speed railway system as a practical example, where the accuracy of our numerical model was successfully validated by experimental results in calculating wear distribution. The subsequent deep learning model demonstrated high accuracy ($R^2 > 0.95$) in predicting future wear depth at distinct positions against ground truth data. This presented approach offers a wide range of applications for predicting the wear evolution of equipment in various engineering fields.

KEYWORDS

contact wire clips, data-driven, machine learning, numerical simulation, wear prediction

1 Introduction

Predicting the wear evolution of metal structural components is of crucial importance in engineering systems for accurately assessing equipment service life. As a primary failure mechanism in mechanical systems, wear not only affects equipment reliability and safety but also directly impacts maintenance costs and economic benefits. Particularly in critical infrastructure sectors such as high-speed railways, aerospace, and energy equipment, precisely predicting the wear behavior of metal components has become a core challenge in engineering practice (Archard, 1953; Bhushan, 2013; Hsu and Shen, 2004; He et al., 2021; Enblom, 2009; Flodin and Andersson, 2001; Liu et al., 2025; Karakurt et al., 2024). Recent research has demonstrated significant advancements in enhancing wear resistance through strategic material design, including ceramic particle reinforcement, nanoparticle incorporation, and thermal processing optimization. These approaches effectively modify microstructures to achieve superior tribological performance and extended component durability. However, translating these material innovations into practical wear prediction models remains challenging due to complex material behaviors and interfacial interactions that require extensive validation across diverse operating conditions (Sager et al., 2022; Nama et al., 2023; Karaca et al., 2024). This challenge is often compounded by long experimental cycles, high costs, and difficulties in numerical

simulation, which severely restrict prediction accuracy and practical applicability (Bucca and Collina, 2009; Hsu et al., 1997; Shah et al., 2025). The Finite Element Method (FEM) demonstrates significant potential in the field of metal wear prediction. Gonzalez utilized finite element analysis to determine critical wear levels of contact wires in urban rail transit, providing an important foundation for catenary system design optimization (González et al., 2008). Wei et al. proposed a wear calculation model for metro rigid catenary conductors and pantograph strips. By analyzing wear distribution and conductor layout, Wei et al. achieved accurate wear prediction, providing a scientific basis for extending equipment lifespan, developing differentiated maintenance strategies, and optimizing conductor arrangements (Wei et al., 2020). The core advantage of FEM lies in its ability to accurately consider the influence of contact pressure distribution, material property variations, and complex geometric shapes on wear behavior, thereby offering a more precise physical foundation for wear prediction (Liu et al., 2018; Najeh et al., 2021; Wang et al., 2024). For instance, Kim et al. proposed a numerical simulation method for predicting oscillating metal contact wear by utilizing wear rates measured from pin-disk tribometer tests as inputs. Their computational results demonstrated excellent agreement with block-ring experiments, effectively reducing computational costs (Kim et al., 2005). Similarly, Bose et al. developed an FEM-based sliding wear prediction method for rail materials by obtaining contact pressures at contact nodes and combining them with the Archard wear model to calculate wear volume (Bose and Ramkumar, 2019). Nevertheless, traditional finite element simulation still faces significant challenges, particularly low computational efficiency and difficulties in model parameter calibration, when dealing with wear evolution under long-term cyclic loading (Kužnar and Lorenc, 2021; González et al., 2008; Springis and Boiko, 2025). Specifically, in practical engineering problems requiring the simulation of millions of load cycles, the computational costs often become prohibitive, which greatly limits the widespread application of FEM in engineering practice (Bi, 2017; Rao, 2010; Marinkovic and Zehn, 2019).

In recent years, data-driven methods combined with deep learning have been widely used in diverse engineering. Liu et al. proposed a Bézier curve-based nonuniform hollow strut design for body-centered cubic lattices, achieving 92.8% higher stiffness and 99.6% greater strength than benchmark structures while maintaining target density through deep learning optimization (Liu et al., 2025). Zhou et al. achieved spatial tuning of positive-negative Poisson's ratio behavior in two dimensional rec-tangular perforated materials through gradient design combined with deep learning and meta heuristic algorithms, enabling precise control over material deformation (Zhou et al., 2024). Mulder et al. developed a machine learning framework addressing measurement errors to predict contact wire wear rates, achieving ± 0.12 mm thickness prediction accuracy over 4 years with 95% confidence (Mulder et al., 2025). Chen et al. applied Partial Least Squares Regression to predict bearing wear in steel production with limited sensor data, achieving 90% prediction accuracy and enabling condition based maintenance instead of fixed 4 week replacement cycles (Chen et al., 2021). Kollu and Kittur systematically reviewed deep learning applications in mechanical engineering from 2015 to 2024, demonstrating 10%–35% accuracy

improvements over conventional machine learning and physics based approaches in fault diagnosis and predictive maintenance (Kollu and Kittur, 2025). Karaduman et al. developed a convolutional neural network architecture combined with Hough transform and power law transformation to process 909 pantograph images. Experiments showed that this model outperforms classical architectures such as ResNet50 and VGG16 in current collector strip wear detection, providing a more reliable monitoring solution for railway power transmission safety (Karaduman and Akin, 2020). In the field of engineering wear prediction, research has begun exploring the integration of machine learning methods with physical models to enhance prediction accuracy and computational efficiency (Hu et al., 2024; Karniadakis et al., 2021; Pashmforoush et al., 2024; Hao et al., 2023; Li et al., 2022). However, the existing works mainly depend on data analysis, and lack analysis of wear evolution, which fails to find key factors control wear evolution, and therefore, a large number of data is required in prediction.

In railway system, the wear behavior of key components in high-speed railway power supply systems directly affects the safety and reliability of train operations (Li et al., 2023; Wu et al., 2023). Usuda established a contact wire wear prediction model by measuring pantograph contact force, off-line arcing, and current collection on commercial Shinkansen lines. This model revealed that wear in high current regions is primarily influenced by arcing, while wear in low current regions is dominated by contact force (Usuda et al., 2011). Collina et al. proposed a method combining pantograph-catenary dynamic interaction simulation with wear models to predict railway contact wire wear. This model considers both electrical and mechanical factors, effectively tracking the evolution of contact wire pro-file with increasing pantograph passes (Collina et al., 2002). Liu et al. systematically reviewed research progress in high-speed railway catenary systems across four aspects: equilibrium state solving, dynamic modeling, noncontact detection, and evaluation methods. They proposed that multiobjective constraint structural methods and nonlinear finite element techniques could enhance catenary safety and detection accuracy (Liu et al., 2018). Additionally, traditional experimental methods require extensive cyclic testing, which is not only time consuming and labor intensive but also difficult to accurately reproduce actual operating conditions, further exacerbating the challenges of wear prediction.

This study proposes a simulation-driven deep learning prediction framework, aiming to achieve high-precision prediction of wear evolution in metal structural components. The core innovation of this framework lies in the organic combination of high-precision finite element modeling with deep learning technology, where the finite element simulation provides accurate wear mechanism analysis and training data, while the data-driven model captures complex nonlinear evolution patterns and long-term prediction capabilities. For application perspective, we selected high-speed railway contact wire clips as a typical case study due to their representative wear behavior and severe consequences upon failure. Specifically, our methodology comprises four key steps (Figure 1): First, a simplified geometric model of high-speed railway catenary contact wire clips is established based on actual dimensions; second, a high-precision finite element model is developed to accurately simulate the contact mechanics behavior and wear distribution

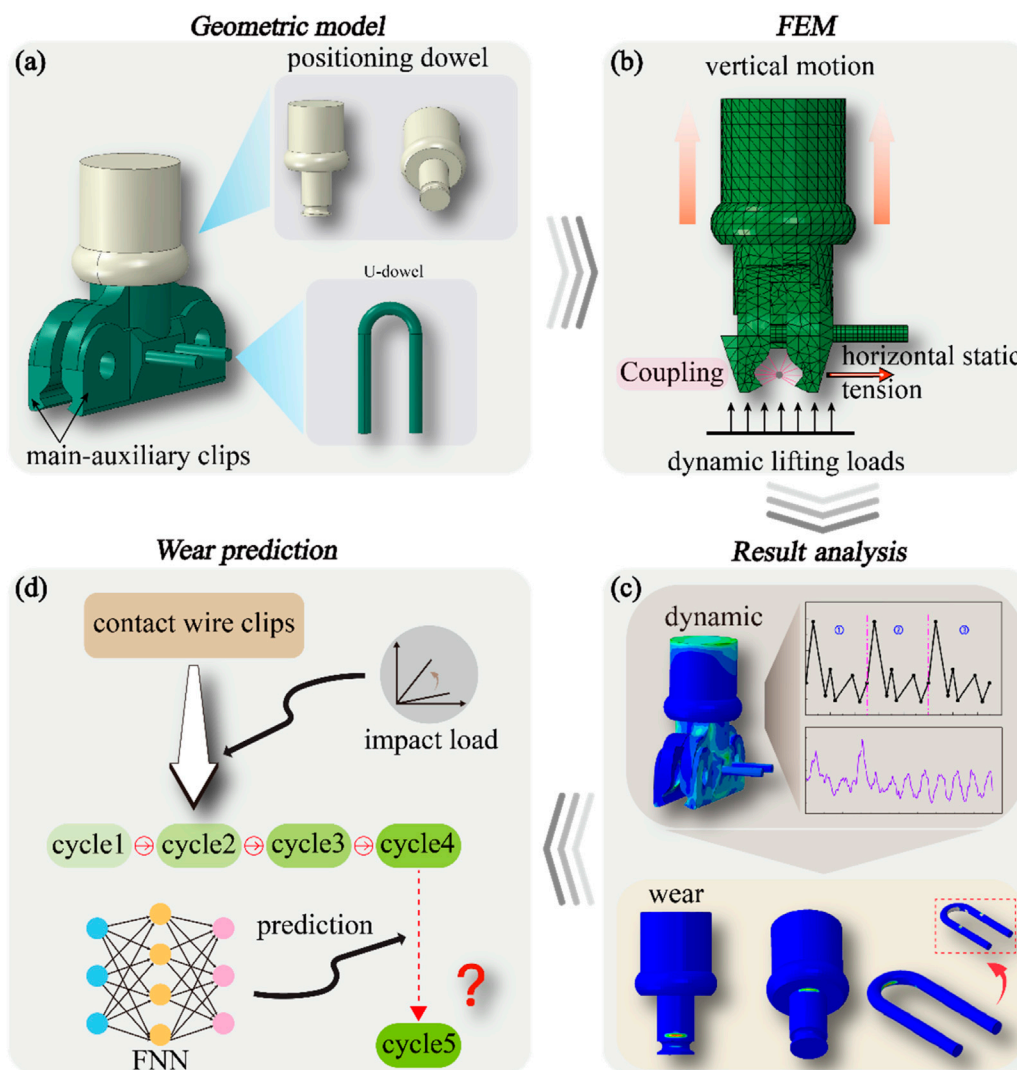


FIGURE 1 Schematic diagram of structural wear prediction method. (a) geometric structure of contact wire clips, (b) finite element models, (c) simulation results, (d) prediction of wear evolution based on deep learning.

characteristics of the contact wire clips under dynamic loading conditions; third, the wear evolution mechanism of components under dynamic service conditions is systematically elucidated; finally, based on finite element simulation results, a deep learning model is trained that can predict wear depth distribution at any future time using applied loads and wear evolution data. By comparing experimental measurements with numerical simulation results, the accuracy of the finite element model in calculating wear distribution was verified. The trained deep learning model demonstrates excellent performance in predicting future wear depth at different positions, with R^2 values exceeding 0.95, significantly outperforming traditional methods. Compared to purely data-driven approaches that typically require thousands of operational samples for stable convergence, our simulation-driven framework achieves high prediction accuracy ($R^2 > 0.95$) with only 200 finite element simulations, reducing data demand by over 80%. Relative to traditional physical models that necessitate full-cycle finite element analysis for each prediction

(computationally prohibitive for long-term forecasting), the trained deep learning model delivers millisecond-level inference while maintaining comparable physical fidelity. This balanced integration yields a 4%–6% accuracy improvement over classical machine learning baselines (e.g., Random Forest) with significantly lower computational overhead.

2 Models and methods

2.1 Finite element model

As shown in Figure 1a, the contact wire clips consist of three core components: main and auxiliary clamp plates, positioning dowel, and U-dowel. As the primary load-bearing component, the main clamp plate is hinged to the positioning dowel via a dual-lug structure and subjected to horizontal tensile forces from the contact wire ranging

TABLE 1 Material properties of components.

Material	Density ρ (kg/m ³)	Poisson's ratio ν	Elastic modulus E, GPa
CuNi ₂ Si	8,900	0.34	120
AlSi ₇ Mg _{0.6}	2,600	0.33	70

from 80 to 3000 N. The auxiliary clamp plate cooperates with the main clamp plate to form an enclosed clamping cavity that secures the contact wire. The positioning dowel, as part of the positioning assembly, is inserted into the sleeve of the main clamp plate to constrain vertical movement. The U-dowel features a U-shaped cylindrical design and passes through the alignment holes of both the main and auxiliary clamp plates to restrict lateral displacement of the plates. To accurately simulate the mechanical behavior, a three-dimensional geometric model was constructed based on actual engineering dimensions and assembly relationships. In terms of material selection, CuNi₂Si material was used for the main and auxiliary clamp plates as well as the U-dowel (green components in Figure 1a), while AlSi₇Mg_{0.6} material was selected for the positioning dowel (gray-white components in Figure 1a). The material parameters are presented in Table 1.

The original geometric model was simplified, and a hybrid meshing method was adopted, where tetrahedral unstructured elements were used for geometrically irregular components, while hexahedral structured elements were combined for regular regions. To ensure accuracy in high stress gradient areas, refined meshing with element size of 1 mm was applied around the contact area of the U-dowel. The body regions of the main and auxiliary clamp plates were meshed with 3 mm transition elements to balance computational efficiency and solution accuracy, as shown in Figure 1b. Multi-point constraint (MPC) was utilized to equivalently model bolted connections. Key parameters of the Archard wear model—including friction coefficient $\mu = 0.55$, wear coefficient $K = 8.8 \times 10^{-12} \text{ m}^3/(\text{Nm})$, and material hardness $H = 200 \text{ HV}$ —were calibrated based on friction and wear tests for the copper-steel tribopair following the ASTM G99 standard. A graded loading strategy was employed: Step 1, initial equilibrium stage, where full constraint boundary conditions ($U_1 = U_2 = U_3 = 0$) were applied to fix the positioning dowel, and horizontal tensile forces were applied along the contact wire axis on the inner side of the main clamp plate; the tensile forces were selected as 80 N and 3000 N, while the gravity field module was used to automatically calculate the influence of device self-weight; Step 2, dynamic response stage, where the vertical degree of freedom of the positioning dowel was released, and two types of vertical dynamic loads were applied at the bottom of the clamp plates.

2.2 Finite element calculation method for wear

This study adopts the classical Archard wear model as the theoretical foundation. Its basic form is expressed as Equation 1:

$$V = K \cdot \frac{F \cdot l}{H} \quad (1)$$

where V represents the volumetric wear of the material (unit: m³), F is the normal load (N), l is the relative sliding distance (m), H

represents the Brinell hardness of the softer material (Pa), and K is the dimensionless wear coefficient. This model reveals the linear relationship between wear volume and contact load as well as sliding distance. By simplifying the contact area projection to unit area A , the wear depth per unit area (also referred to as “wear distance”) can be expressed as Equation 2:

$$w_l = \frac{K \cdot p \cdot l}{H} \quad (2)$$

In practical engineering applications, the Archard model is typically extended to adapt to complex operating conditions. Considering the significant influence of friction behavior on wear in high-speed railway contact systems, this study adopts an extended model that incorporates friction coefficient. By differentiating with respect to time, the wear rate for numerical simulation is expressed as Equation 3:

$$\dot{w}_l = \frac{K \cdot \mu \cdot p \cdot \|\dot{\gamma}\|}{H} \quad (3)$$

In the equation, \dot{w}_l represents the wear depth rate per unit time (m/s), μ is the friction coefficient; p denotes the contact pressure (Pa), and $\|\dot{\gamma}\|$ is the relative sliding speed on the contact surface (m/s).

In simulation process, a step or sequence of steps can be repeated until termination criteria are met. Figure 2 illustrates the repetition of step sequences, where each sequence represents a batch of physical wear cycles until stopping conditions are satisfied. Each slender rectangle in the figure corresponds to a physical wear cycle, enumerated along the horizontal axis. The vertical axis represents the simulation time for each wear cycle, and the rectangles maintain the same height due to the repetitive loading history. Solid rectangular bars represent directly simulated wear cycles and indicate the approximate effect of a group of physical cycles, scaled according to the wear coefficient of the represented number of physical cycles. A group of dashed rectangles adjacent to the solid lines represents physical wear cycles that are not directly simulated. Depending on the batch size, accurate wear prediction associated with a large number of physical cycles can be achieved by simulating only a few representative cycles.

The entire process is divided into several cycles, where the wear in each cycle is estimated using a single representative physical wear event. The calculated nodal displacements and other data from one cycle serve as the initial conditions for subsequent cycles, enabling dynamic adjustment of the wear coefficient for the next cycle, and so forth. In this study, Step 2 is defined as the wear cycle step, with the total number of cycles set to 10 and the batch size set to 500, thereby enabling the simulation of wear evolution over 5,000 physical cycles under different tensile loads.

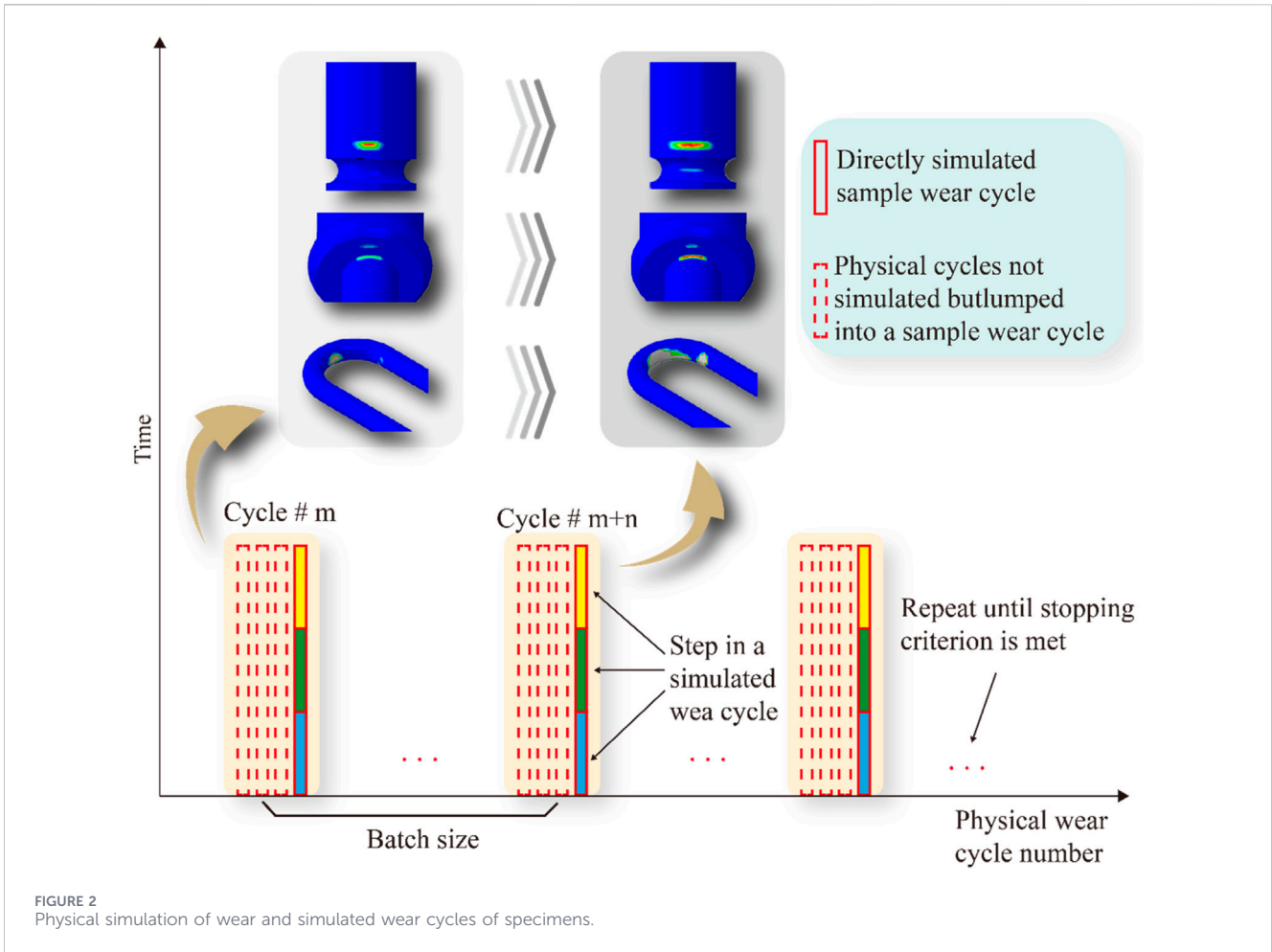


FIGURE 2 Physical simulation of wear and simulated wear cycles of specimens.

2.3 Deep learning-based wear prediction method

Let the input feature vector be $x \in \mathbb{R}^d$ (where d represents the feature dimension), and the target wear depth be a scalar $y \in \mathbb{R}$. To eliminate dimensional differences and accelerate model convergence, standardization processing is applied separately to the input features and target variables (Equation 4):

$$x_{\text{norm}} = \frac{x - \mu_x}{\sigma_x}, y_{\text{norm}} = \frac{y - \mu_y}{\sigma_y} \quad (4)$$

where μ_x, σ_x and μ_y, σ_y represent the mean vectors and standard deviations of the features and target variables in the training set, respectively. During the prediction stage, the original scale is recovered through inverse transformation (Equation 5):

$$\hat{y} = \hat{y}_{\text{norm}} \cdot \sigma_y + \mu_y \quad (5)$$

\hat{y}_{norm} represents the standardized prediction value output by the model.

A fully connected feedforward neural network was constructed for the prediction model, with the ReLU function selected as the activation function. The output layer employed linear activation to directly regress the wear depth values. The loss function was defined

as the mean squared error (MSE) between the predicted values and the true values (Equation 6):

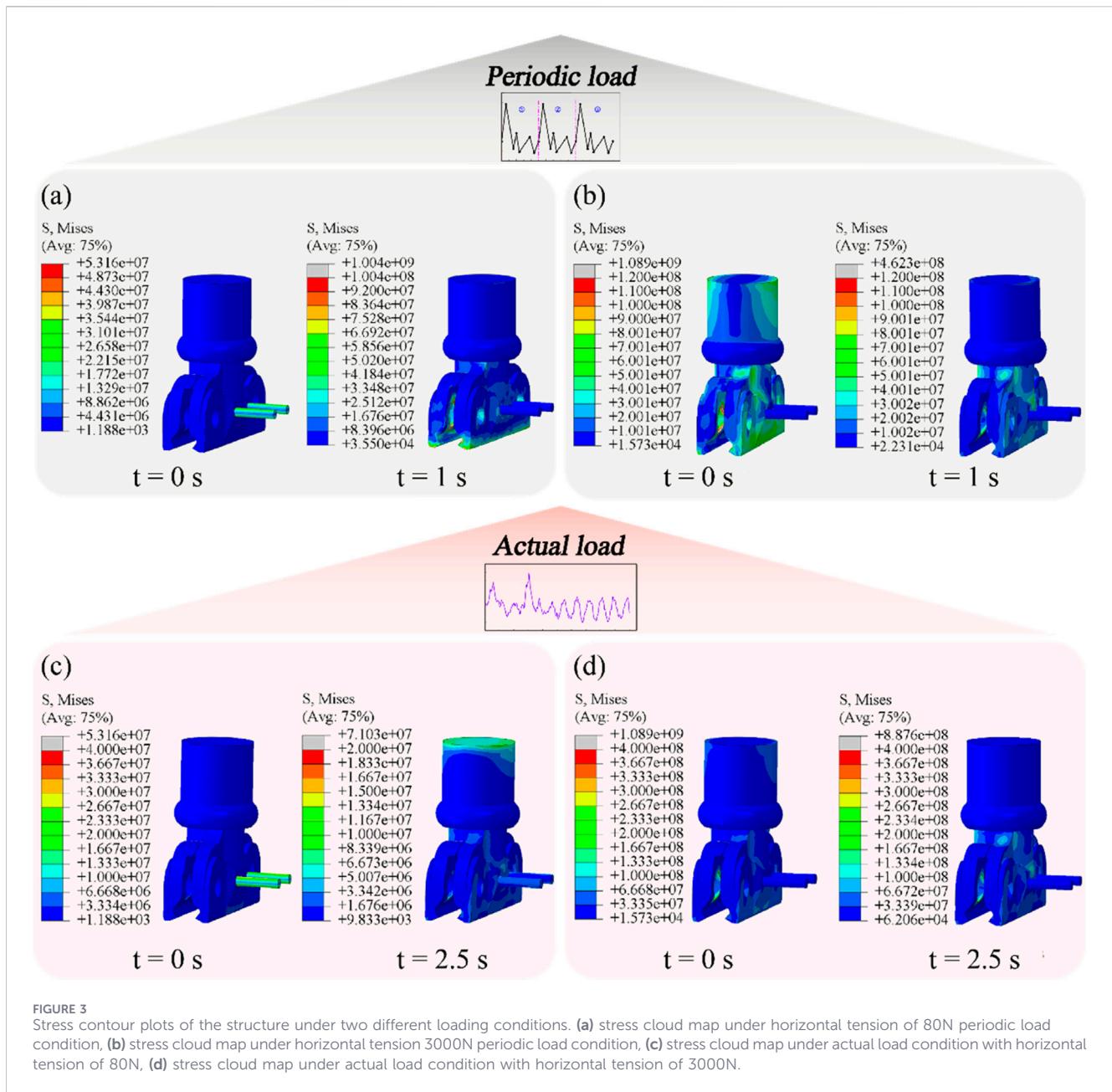
$$\mathcal{L} = \frac{1}{N} \sum_{i=1}^N (\hat{y}_{\text{norm}}^{(i)} - y_{\text{norm}}^{(i)})^2 \quad (6)$$

where N represents the number of training samples. Network parameters are optimized through Adam to minimize \mathcal{L} . An early stopping mechanism is introduced during the training process to prevent overfitting: when the validation set loss fails to decrease for several consecutive epochs, training is terminated and the model with the best validation performance is saved.

3 Results and discussion

3.1 Correlation between structural dynamic response and wear

There exists a close intrinsic correlation between structural dynamic response and wear behavior. Through finite element simulation analysis, the stress distribution generated in various components under dynamic excitation when the pantograph passes can be clearly observed, which directly determines the wear distribution pattern at the contact interface. Critical areas



such as the hinge region between the main and auxiliary clamp plates, and the contact interface between the U-dowel and clamp plate hole wall, often form significant stress concentration zones due to geometric discontinuities and the concentrated effect of load transfer paths. As shown in Figures 3a,c, at the initial stage under low tensile force levels, when the structure is subjected to vertical lifting force instantaneously, the stress value of the U-dowel (which serves as the connecting component between the main clamp plate, auxiliary clamp plate, and positioning dowel) suddenly increases and becomes significantly higher than other areas. With increased tensile force, the regions with initially high stress shift from the U-dowel to the main clamp plate, auxiliary clamp plate, and positioning dowel. These regions not only exhibit higher contact pressure and local strain, but also accompany more intense microscopic material

removal processes. The spatial distribution characteristics of dynamic response show high spatial correlation with the ultimate wear morphology. During dynamic service, the wear evolution of the structure is not uniformly distributed, but is closely related to the stress distribution and relative sliding characteristics under load. When external dynamic loads act on the bottom of the clamp plates, through the clamping action of the main and auxiliary clamp plates, the load is transmitted to the contact interface between the U-dowel and clamp plate hole wall, forming a complex contact pressure field. The spatial distribution characteristics of this pressure field directly determine the initial position and propagation path of wear. Furthermore, the geometric constraints of the structure also significantly influence wear behavior. For example, at the mating interface between the positioning dowel and the main clamp

plate sleeve, microamplitude relative sliding occurs under dynamic loads due to assembly clearance. Through the cumulative effect revealed by the Archard wear model, characteristic wear grooves are formed.

Through in-depth analysis of the spatial coupling relationship between dynamic response and wear, “wear-sensitive zones” within the structure can be identified, providing scientific basis for optimizing structural design and developing targeted maintenance strategies. Finite element simulation results reveal that the mating area between the positioning dowel and sleeve, along with the contact interface between the U-dowel and clamp plate hole wall, these represent the two most critical areas with severe wear, as shown in Figure 4c. The common characteristics of these regions are high contact pressure and significant relative sliding, with their dynamic response features showing a clear correspondence to wear depth distribution.

3.2 Effect of external loads and impact velocity on wear evolution

External load serves as a key factor influencing the wear behavior of contact wire clips, with its mechanism exhibiting significant nonlinear characteristics. The relationship between wear depth and horizontal tensile load is not simply linear, but rather features an optimal load interval. At lower load levels, insufficient clamping force results in substantial relative sliding at the contact interface, leading to accelerated wear. As the load increases (As shown in Figure 4), the clamping effect strengthens, reducing the amplitude of relative sliding and consequently decreasing wear severity. However, when the load exceeds a certain critical value, excessive contact pressure reaccelerates the material removal process. This non-monotonic variation pattern reveals the complexity of the load-wear relationship, indicating that structural design requires identification of the optimal operating load range. Wear evolution processes under different load levels exhibit similar dynamic characteristics, where wear rate shows an initial increase followed by a decrease as the number of cycles progresses. This phenomenon can be attributed to the adaptive evolution of contact interface morphology during wear: initial wear expands the contact area, leading to more uniform stress distribution and gradually reduced wear rate. Simultaneously, the accumulation of wear debris at the contact interface forms a protective layer that further slows down subsequent wear processes.

The influence of impact velocity on wear evolution is primarily reflected in the alteration of wear dynamics characteristics. Under identical horizontal tensile force conditions, as impact velocity increases, not only does the ultimate wear depth significantly increase, but the wear evolution pattern also undergoes noticeable transformation. In low-velocity impact conditions, the wear process remains relatively gentle, with wear depth increasing slowly with the number of cycles, reflecting a stable wear mechanism of materials under low strain rates. At medium impact velocities, the wear curve exhibits nonlinear characteristics with an initial rapid increase followed by deceleration, indicating dynamic adjustment of the interfacial contact state during the wear process. Under high-velocity impact conditions, the wear rate substantially increases while

remaining relatively constant, presenting an almost linear evolution trend. This velocity dependency can be explained from a contact dynamics perspective: increased impact velocity leads to higher numbers of load cycles per unit time, while simultaneously increasing the instantaneous contact force during each impact. These two factors jointly accelerate the accumulation of fatigue damage in the material. Additionally, at high impact velocities, the contact interface lacks sufficient time to form a stable wear debris layer that could provide protective effects, which constitutes another crucial reason for the sustained high wear rate. By comparing finite element simulation results with actual experimental data, high consistency can be observed in both wear location and distribution morphology, validating the reliability of the numerical model.

3.3 Wear prediction

A specific prediction model was constructed for the wear evolution process at critical locations. To accurately characterize the wear behavior of the U-dowel region, 200 independent finite element simulations were conducted under distinct initial conditions or loading scenarios. The sample size was determined through preliminary convergence analysis, which confirmed that 200 simulations with uniformly distributed impact velocities adequately cover the parameter space of practical service conditions and yield stable prediction performance. Two representative monitoring points were selected from the component, with each point capturing a complete wear evolution trajectory—from the initial state to the fifth wear cycle—derived from each of the 200 independent simulations. Each sample consists of six parameters: impact velocity $V1$ and the corresponding wear depth values for five consecutive wear cycles (C1-C5). The impact velocity $V1$ is uniformly distributed within the range of 0.1000–2.0000 m/s, sufficiently covering the dynamic load conditions that contact wire clips may encounter during actual service. The network input is designed as a five-dimensional feature vector $[V1, C1, C2, C3, C4]$, with the output being the predicted wear depth $C5$ for the fifth cycle. Regarding the network architecture design, as shown in Figure 5a, a three-layer fully connected neural network structure is adopted, with an input layer dimension of 5, sequentially passing through hidden layers of 64 and 32 dimensions, and finally outputting a single-dimensional prediction value. The ReLU nonlinear transformation is selected as the activation function for hidden layers to ensure the model has sufficient expressive capability to capture the complex nonlinear characteristics of wear evolution. During the training process, mean squared error is used as the loss function, with the Adam optimizer performing parameter updates, an initial learning rate set to 0.001, and an early stopping mechanism implemented to prevent overfitting, terminating training when validation loss shows no improvement for 10 consecutive epochs. The dataset is divided into a training set (180 samples) and a testing set (20 samples). Before training, all features undergo standardization processing, adjusting the mean to 0 and standard deviation to 1, to accelerate convergence and improve model stability. Furthermore, the testing set achieves a prediction accuracy of over 95%, indicating that the current sample size provides sufficient representation of wear evolution patterns under practical operating conditions.

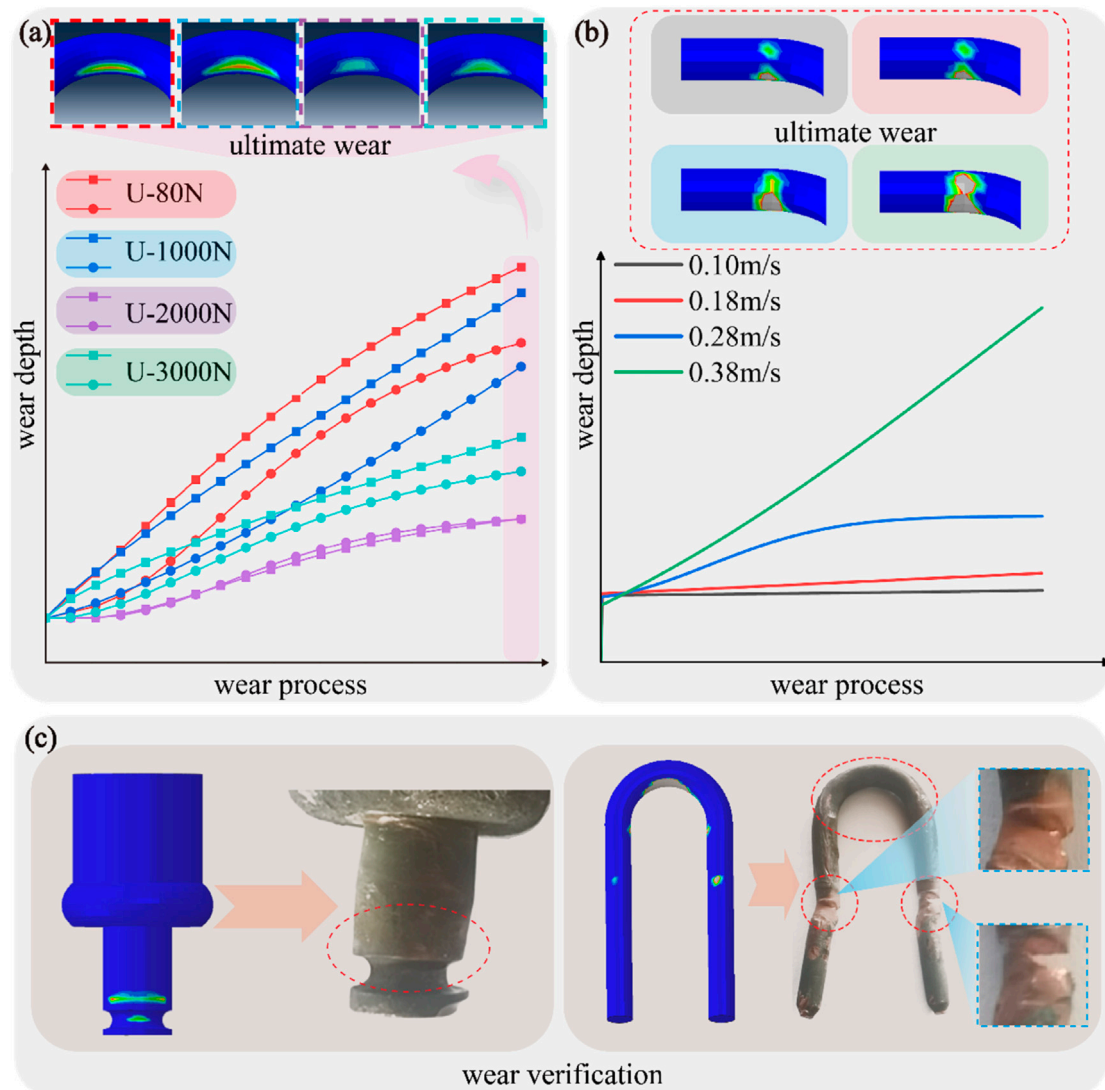


FIGURE 4 Factors influencing structural wear evolution. (a) wear process and wear depth curve under different tensile periodic load conditions, (b) wear process and wear depth curve under different impact velocities, (c) finite element and experimental comparison.

To further validate the superiority of the proposed fully connected neural network, a comparison with the classical machine learning method Random Forest (RF) was conducted under identical training/testing splits and input features. As summarized in Table 2, while RF achieves respectable performance ($R^2 > 0.85$), the deep learning model consistently outperforms it by 4%–6% in R^2 and reduces prediction error by approximately 50%. This advantage stems from the network's stronger capacity to capture the nonlinear temporal dependencies in wear evolution trajectories, which tree-based methods struggle to model effectively with limited samples. The prediction results demonstrate that the deep learning model exhibits excellent predictive performance at both monitoring positions. As shown in Figure 5b, the scatter plot between actual wear depths and predicted values is tightly distributed near the diagonal line, with correlation coefficients R^2 reaching 0.951 and 0.975 respectively, indicating the model's highly accurate capability in capturing wear

evolution trends. Compared to traditional physical models, this data-driven approach demonstrates significant advantages in computational efficiency. This efficiency improvement makes real-time wear monitoring and life prediction possible.

To validate that the deep learning model provides meaningful improvement beyond trivial predictions, we compared its performance against two simple baselines using the same 20 testing samples: (1) Persistence: directly using the previous wear depth as prediction; (2) Linear extrapolation: fitting a linear trend to C_1 – C_4 and extrapolating to C_5 . Results are summarized in Table 2.

Relative MSE is normalized by the MSE of the persistence baseline. The proposed model reduces prediction error by 85% compared to the simplest baseline and by approximately 50% relative to Random Forest, confirming its non-trivial contribution and superior capability in capturing complex nonlinear wear evolution patterns.

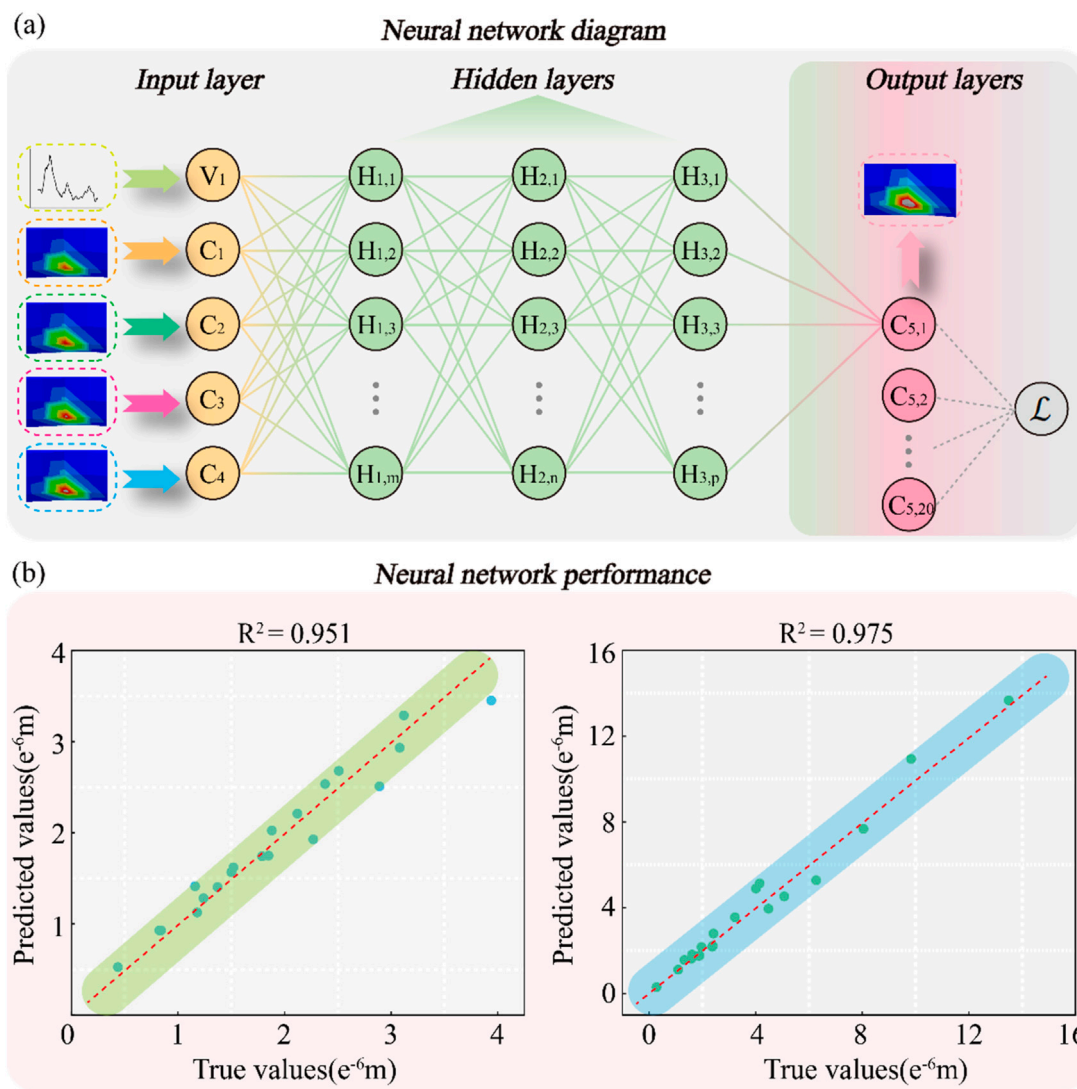


FIGURE 5 Schematic diagram of neural network for predicting ultimate wear based on wear evolution. (a) schematic diagram of neural network, (b) R^2 plot of true value and predicted value.

4 Conclusion

This study proposes a simulation-driven deep learning prediction framework for accurately predicting wear evolution behavior of metal structural components under dynamic service conditions. The research reveals a strong intrinsic coupling

relationship between structural dynamic response and wear distribution, where wear does not occur uniformly but is highly concentrated in stress concentration regions and contact interfaces with significant relative sliding. This provides theoretical basis for identifying critical wear-sensitive zones. Horizontal tensile load and impact velocity exhibit complex nonlinear influence patterns on wear evolution. The relationship between wear depth and horizontal tensile force shows non-monotonic characteristics with an optimal load operating range. Increasing the impact velocity not only raises the ultimate wear depth but also transforms the wear evolution pattern from a nonlinear decay to an approximately linear growth. This change stems from the dynamic evolution of the contact dynamics characteristics and interface states. Leveraging the wear mechanisms identified through numerical simulation, the constructed deep learning prediction model achieves excellent performance in capturing wear evolution patterns by integrating

TABLE 2 Prediction performance comparison with trivial baselines (testing set, $n = 20$).

Method	R2 (Point1)	R2 (Point1)	Relative MSE
Persistence	0.62	0.68	1 (ref)
Linear extrapolation	0.76	0.82	0.61
Random forest	0.89	0.91	0.32
Our model	0.951	0.975	0.15

simulation-derived mechanisms with data features. This model significantly overcomes limitations of traditional methods such as low computational efficiency and difficulties in long-term prediction, achieving a technological transition from “periodic maintenance” to “predictive maintenance.” The framework possesses excellent universality and scalability, being applicable not only to high-speed railway contact wire clips but also extendable to wear prediction of key components in aerospace, energy equipment, and other fields.

Data availability statement

The original contributions presented in the study are included in the article/supplementary material, further inquiries can be directed to the corresponding author.

Author contributions

HZ: Methodology, Investigation, Writing – original draft, Conceptualization. QZ: Software, Methodology, Writing – review and editing, Validation. YZ: Conceptualization, Funding acquisition, Validation, Writing – review and editing, Supervision. BZ: Investigation, Writing – review and editing, Validation, Software. MZ: Software, Investigation, Validation, Writing – review and editing. CL: Software, Investigation, Validation, Writing – review and editing.

Funding

The author(s) declared that financial support was received for this work and/or its publication. The author of this article sincerely thanks the National Nature Science Foundation of China

References

- Archard, J. F. (1953). Contact and rubbing of flat surfaces. *J. Applied Physics* 24 (8), 981–988. doi:10.1063/1.1721448
- Bhushan, B. (2013). *Principles and applications of tribology*. John Wiley & Sons: Chichester, West Sussex, United Kingdom.
- Bi, Z. (2017). *Finite element analysis applications: a systematic and practical approach*. Academic Press.
- Bose, K. K., and Ramkumar, P. (2019). Finite element method based sliding wear prediction of steel-on-steel contacts using extrapolation techniques. *Proc. Institution Mech. Eng. Part J J. Eng. Tribol.* 233 (10), 1446–1463. doi:10.1177/1350650119836813
- Bucca, G., and Collina, A. (2009). A procedure for the wear prediction of collector strip and contact wire in pantograph–catenary system. *Wear* 266 (1-2), 46–59. doi:10.1016/j.wear.2008.05.006
- Chen, X., Van Hillegerberg, J., Topan, E., Smith, S., and Roberts, M. (2021). Application of data-driven models to predictive maintenance: bearing wear prediction at TATA steel. *Expert Systems Applications* 186, 115699. doi:10.1016/j.eswa.2021.115699
- Collina, A., Melzi, S., and Facchinetti, A. (2002). On the prediction of wear of contact wire in OHE lines: a proposed model. *Veh. System Dynamics* 37 (Suppl. 1), 579–592. doi:10.1080/00423114.2002.11666264
- Enblom, R. (2009). Deterioration mechanisms in the wheel–rail interface with focus on wear prediction: a literature review. *Veh. Syst. Dyn.* 47 (6), 661–700. doi:10.1080/00423110802331559
- Flodin, A., and Andersson, S. (2001). A simplified model for wear prediction in helical gears. *Wear* 249 (3-4), 285–292. doi:10.1016/S0043-1648(01)00556-7
- González, F. J., Chover, J. A., Suarez, B., and Vázquez, M. (2008). Dynamic analysis using finite elements to calculate the critical wear section of the contact wire in suburban railway overhead conductor rails. *Proc. Institution Mech. Eng. Part F J. Rail Rapid Transit* 222 (2), 145–157. doi:10.1243/09544097JRR1144
- Hao, C., Mao, X., Ma, T., He, S., Li, B., Liu, H., et al. (2023). A novel deep learning method with partly explainable: intelligent milling tool wear prediction model based on transformer informed physics. *Adv. Eng. Inf.* 57, 102106. doi:10.1016/j.aei.2023.102106
- He, Z., Shi, T., Xuan, J., and Li, T. (2021). Research on tool wear prediction based on temperature signals and deep learning. *Wear* 478, 203902. doi:10.1016/j.wear.2021.203902
- Hsu, S. M., and Shen, M. (2004). Wear prediction of ceramics. *Wear* 256 (9-10), 867–878. doi:10.1016/j.wear.2003.11.002
- Hsu, S. M., Shen, M. C., and Ruff, A. W. (1997). Wear prediction for metals. *Tribol. Int.* 30 (5), 377–383. doi:10.1016/S0301-679X(96)00067-9
- Hu, H., Qi, L., and Chao, X. (2024). Physics-informed neural Networks (PINN) for computational solid mechanics: numerical frameworks and applications. *Thin-Walled Struct.* 205, 112495. doi:10.1016/j.tws.2024.112495
- Karaca, M., Polat, S., and Esen, I. (2024). Reciprocating dry sliding wear behaviour of BN@MXene/AA7075 composites. *J. Compos. Mater.* 15 (18), 2007–2026. doi:10.1177/00219983241257665
- Karaduman, G., and Akin, E. (2020). A deep learning based method for detecting of wear on the current collector strips’ surfaces of the pantograph in railways. *IEEE Access* 8, 183799–183812. doi:10.1109/ACCESS.2020.3029555

(52472421) and the China Academy of Railway Sciences Fund Project (2024YJ288) and the China Tianjin Province Scientific Research Project (24ZYCGYS00800) for their funding of this article.

Conflict of interest

Authors HZ, QZ, YZ, and BZ were employed by Standards & Metrology Research Institute, China Academy of Railway Sciences Corporation Limited. BZ was employed by the company China Railway Test & Certification Center Limited.

The remaining author(s) declared that this work was conducted in the absence of any commercial or financial relationships that could be construed as a potential conflict of interest.

Generative AI statement

The author(s) declared that generative AI was not used in the creation of this manuscript.

Any alternative text (alt text) provided alongside figures in this article has been generated by Frontiers with the support of artificial intelligence and reasonable efforts have been made to ensure accuracy, including review by the authors wherever possible. If you identify any issues, please contact us.

Publisher’s note

All claims expressed in this article are solely those of the authors and do not necessarily represent those of their affiliated organizations, or those of the publisher, the editors and the reviewers. Any product that may be evaluated in this article, or claim that may be made by its manufacturer, is not guaranteed or endorsed by the publisher.

- Karakurt, V., Esen, I., Zığünder, O., and Turen, Y. (2024). Investigation of mechanical, electrical conductivity, wear and corrosion performances of traditional CuNi2Si and new high performance CuNiCoSi copper based alloys. *Can. Metall. Q.* 64 (3), 1122–1148. doi:10.1080/00084433.2024.2425495
- Karniadakis, G. E., Kevrekidis, I. G., Lu, L., Perdikaris, P., Wang, S., and Yang, L. (2021). Physics-informed machine learning. *Nat. Rev. Phys.* 3 (6), 422–440. doi:10.1038/s42254-021-00314-5
- Kim, N. H., Won, D., Burris, D., Holtkamp, B., Gessel, G. R., Swanson, P., et al. (2005). Finite element analysis and experiments of metal/metal wear in oscillatory contacts. *Wear* 258 (11–12), 1787–1793. doi:10.1016/j.wear.2004.12.014
- Kollu, G. S., and Kittur, J. (2025). Integrating deep learning into mechanical engineering: a systematic review of applications and educational implications. *Comput. Appl. Eng. Educ.* 33 (3), e70048. doi:10.1002/cae.70048
- Kužnar, M., and Lorenc, A. (2021). A method of predicting wear and damage of pantograph sliding strips based on artificial neural networks. *Materials* 15 (1), 98. doi:10.3390/ma15010098
- Li, Y., Wang, J., Huang, Z., and Gao, R. X. (2022). Physics-informed meta learning for machining tool wear prediction. *J. Manuf. Syst.* 62, 17–27. doi:10.1016/j.jmsy.2021.10.013
- Li, L., Mahmoodian, M., and Khaloo, A. (2023). Service life prediction of worn contact wires under multiple failure modes. *Struct. Infrastructure Eng.* 19 (11), 1530–1541. doi:10.1080/15732479.2022.2035405
- Liu, Z., Song, Y., Han, Y., Wang, H., Zhang, J., and Han, Z. (2018). Advances of research on high-speed railway catenary. *J. Modern Transportation* 26 (1), 1–23. doi:10.1007/s40534-017-0148-4
- Liu, Y., Wei, Q., Wang, W., Zhao, L., and Hu, N. (2025). Multiscale modeling and data-driven life prediction of kinematic interface behaviors in mechanical drive systems. *Coatings* 15 (6), 660. doi:10.3390/coatings15060660
- Marinkovic, D., and Zehn, M. (2019). Survey of finite element method-based real-time simulations. *Appl. Sci.* 9 (14), 2775. doi:10.3390/app9142775
- Mulder, J., Vahdatikhaki, F., Yin, X., Vermeulen, F., and Voordijk, H. (2025). Predicting the wear rate and thickness of train contact wire using data-driven modelling. *Appl. Sci.* 15 (17), 9362. doi:10.3390/app15179362
- Najeh, T., Lundberg, J., and Kerrouche, A. (2021). Deep-learning and vibration-based system for wear size estimation of railway switches and crossings. *Sensors* 21 (15), 5217. doi:10.3390/s21155217
- Nama, H., Esen, I., Ahlatçı, H., and Karakurt, V. (2023). Effect of aging heat treatment on wear behavior and microstructure characterization of newly developed Al7075+Ti alloys. *Materials* 16, 4413. doi:10.3390/ma16124413
- Pashmforoush, F., Araghizad, A. E., and Budak, E. (2024). Physics-informed tool wear prediction in turning process: a thermo-mechanical wear-included force model integrated with machine learning. *J. Manuf. Syst.* 77, 266–283. doi:10.1016/j.jmsy.2024.09.008
- Sager, A., Esen, I., Ahlatçı, H., and Turen, Y. (2022). Dry wear behaviour of the new ZK60/AlN/SiC particle reinforced composites. *Materials* 15, 8582. doi:10.3390/ma15238582
- Shah, R., Pai, N., Thomas, G., Jha, S., Mittal, V., Shirvni, K., et al. (2025). Machine learning in wear prediction. *J. Tribol.* 147 (4), 040801. doi:10.1115/1.4066865
- Springis, G., and Boiko, I. (2025). Comparative analysis of wear models for accurate wear predictions. *Lubricants* 13 (3), 100. doi:10.3390/lubricants13030100
- Usuda, T., Ikeda, M., and Yamashita, Y. (2011). “Prediction of contact wire wear in high speed railways,” in *Proc. the ninth world congress on railway research*, 1–10.
- Wang, S., Xiang, J., Wang, X., Feng, Q., Yang, Y., Cao, X., et al. (2024). A deep learning based surrogate model for reservoir dynamic performance prediction. *Geoenergy Sci. Eng.* 233, 212516. doi:10.1016/j.geoen.2023.212516
- Wei, X. K., Meng, H. F., He, J. H., Jia, L. M., and Li, Z. G. (2020). Wear analysis and prediction of rigid catenary contact wire and pantograph strip for railway system. *Wear* 442, 203118. doi:10.1016/j.wear.2019.203118
- Zhou, X., Liu, X., Zhao, A., Liu, C., and Wu, H. (2024). Spatial tuning of the positive and negative Poisson’s ratio of metamaterials through gradient design. *Thin-Walled Struct.* 205, 112382. doi:10.1016/j.tws.2024.112382